Regular paper

Substrate specificity of glycoside hydrolase family 1 β-glucosidase AtBGlu42 from *Arabidopsis thaliana* and its molecular mechanism

Shu Horikoshi[1], Wataru Saburi[1], Jian Yu[2], Hideyuki Matsuura[1], James R. Ketudat Cairns[3], Min Yao[2], and Haruhide Mori[1] *

[1]Research Faculty of Agriculture, Hokkaido University, Kita 9 Nishi 9, Sapporo 060-8589, Japan.
[2]Faculty of Advanced Life Science, Hokkaido University, Kita 10 Nishi 8, Sapporo 060-0810, Japan.
[3]School of Chemistry, Institute of Science, Suranaree University of Technology, Nakhon Ratchasima, 30000, Thailand.

Correspondence: Haruhide Mori, hmori@chem.agr.hokudai.ac.jp

Running head: Enzymatic and structural analysis of AtBGlu42

Abstract

Plants possess many glycoside hydrolase family 1 (GH1) β-glucosidases, which physiologically function in cell wall metabolism and activation of bioactive substances, but most remain uncharacterized. One GH1 isoenzyme AtBGlu42 in *Arabidopsis thaliana* has been identified to hydrolyze scopolin using the gene deficient plants, but no enzymatic properties were obtained. Its sequence similarity to another functionally characterized enzyme Os1BGlu4 in rice suggests that AtBGlu42 acts on also oligosaccharides. Here, we show that the recombinant AtBGlu42 possesses high k_{cat}/K_m not only on scopolin, but also on various β-glucosides, cellooligosaccharides, and laminarioligosaccharides. Of the cellooligosaccharides, cellotriose is the most preferred. The crystal structure, determined at 1.7 Å resolution, suggests that Arg342 gives unfavorable binding to cellooligosaccharides at subsite +3. The mutants R342Y and R342A showed the highest preference on cellotetraose or cellopentaose with increased affinities at subsite +3, indicating that the residues at this position have an important role for chain length specificity.

Keywords: β-Glucosidase, Glycoside hydrolase family 1, Substrate specificity, X-ray crystallography, *Arabidopsis thaliana*

Introduction

β-Glucosidase (EC 3.2.1.21) catalyzes the hydrolysis of β-glucosidic linkages at the non-reducing end of substrates to release D-glucose. This enzyme is ubiquitous in archaea, eubacteria, and eukaryotes, and contributes to the degradation of cell wall, metabolism of glycolipids, and activation of bioactive substances (Ketudat Cairns and Esen 2010; Ketudat Cairns *et al.* 2015). Based on the sequence-based classification of glycoside hydrolases, β-glucosidases are in the glycoside hydrolase families (GHs): GH1, GH2, GH3, GH5, GH30, GH39, and GH116 (Lombard *et al.* 2014). Most of these families, excluding GH3 and GH116, fall into GH Clan A. Clan A enzymes share a $(\beta/\alpha)_8$-barrel catalytic domain. Their catalytic residues acting as general acid/base and nucleophile are Glu residues at the C-terminal of β-strands 4 and 7, respectively (Jenkins *et al.* 1995; Henrissat *et al.* 1995; Rye and Withers 2000).

The substrate specificity of GH1 β-glycosidases is very diverse. Most GH1 enzymes act on β-glucosides, but β-D-fucosides, β-D-galactosides, β-D-xylosides, and β-D-mannosides are also their substrates (Ketudat Cairns and Esen 2010). GH1 enzymes also exhibit a variety of specificities for the aglycone of β-glycosides, and oligosaccharides with different linkages and chain lengths (Opassiri *et al.* 2004; Seshadri *et al.* 2009; Opassiri *et al.* 2010; Rouyi *et al.* 2014). Plant GH1 β-glucosidases act on various β-glucosides of secondary metabolites, including plant hormones such as salicylic acid (Himeno *et al.* 2013), tuberonic acid (Wakuta *et al.* 2010; Wakuta *et al.* 2011), abscisic acid (Lee *et al.* 2006), and gibberellin (Hua *et al.* 2013), benzoxazinoids (Babcock and Esen 1994; Sue, Ishihara and Iwamura 2000), cyanohydrins (Hösel *et al.* 1987), alkaloids (Barleben *et al.* 2007; Xia *et al.* 2012), and phenylpropanoids (Ahn *et al.* 2010; Roepke and Bozzo 2015; Baba, Vishwakarma and Ashraf 2017). The enzymes are probably involved in quantitative regulation of the active forms of those compounds through deglycosylation (Ketudat Cairns *et al.* 2015). Plants possess so many GH1 isoenzymes compared with other organisms (Ketudat Cairns *et al.* 2012). Arabidopsis and rice have 40 and 34 functional genes encoding GH1 enzymes, respectively (Xu *et al.* 2004; Opassiri *et al.* 2006). This multiplicity is possibly associated with the regulation of the various compounds through their

specific expression and substrate specificities of the isoenzymes, although most of their physiological functions remain to be clarified.

A GH1 β-glucosidase from Arabidopsis, AtBGlu42, is likely localized in the cytoplasm because it has no N-terminal signal peptide in its precursor sequence, while the other Arabidopsis GH1 isoenzymes are predicted to possess one (Xu *et al.* 2004). AtBGlu42 is known to be involved in the acquisition of rhizobacteria-induced systemic resistance and iron-uptake through deglycosylation of phenolic compounds, mainly the coumarin β-glucoside, scopolin. These functions were predicted on the basis of expression of the gene and the phenotypes of *AtBGlu42*-modified plants (Zamioudis, Hanson and Pieterse 2014; Stringlis *et al.* 2018). On the other hand, AtBGlu42 shares high sequence identity (64%) with the rice cytosolic GH1 β-glucosidase, Os1BGlu4 (Rouyi *et al.* 2014), which has high hydrolytic activity towards laminaribiose (β1-3-linked) and β1-4-linked cellooligosaccharides of degree of polymerization (DP) 3-4 in addition to β-glucosides such as salicin and esculin. These imply that AtBGlu42 may act on not only scopolin but also various β-glucosides including oligosaccharides.

In this study, we investigated enzymatic characteristics and crystal structure of AtBGlu42 using recombinant enzyme produced in *Escherichia coli*. An amino acid residue discriminating the enzyme from other GH1 β-glucosidases in terms of cellooligosaccharide preference was identified in the three-dimensional structure and verified through the site-directed mutagenesis. The local domain structure determining the spatial location of the residues is also discussed.

Materials and methods

Plant materials

A. thaliana ecotype Columbia was grown on half-strength Murashige and Skoog medium (pH 5.7; Wako Pure Chemical Industries, Osaka, Japan) with 10 g L^{-1} sucrose and 3 g L^{-1} gellan gum (Wako Pure Chemical Industries) for 10 days at 23 °C under 16 h light/8 h dark conditions.

AtBGlu42 expression plasmid

Total RNA was prepared from the seedlings of *A. thaliana* with RNeasy Mini Kit (Qiagen, Hilden, Germany), and cDNA was synthesized with Superscript III First-Strand Synthesis System for RT-PCR (Thermo Fisher Scientific, Waltham, MA, USA). The AtBGlu42 cDNA was amplified by PCR with the primers, 5′-GCTTCTTAAGTCTGTCTCTCTCTTC-3′ (sense) and 5′-ACGAAACACITAGTCAAAATATGAG-3′ (antisense), and PrimeSTAR HS DNA polymerase (Takara Bio, Kusatsu, Japan), followed by reamplification with the primers, 5′-GTGCCACGCGGTTCTATGGCACAGAAGCTTAACTT-3′ (sense, the 15-bp overlap with pET-32a underlined) and 5′-CGCAAGCTTGTCGACTCATTCCTTCTTACCTTTGT-3′ (antisense). The amplified DNA was inserted into the pET-32a vector (Novagen, Darmstadt, Germany) using In-Fusion HD Cloning Kit (Takara Bio). The linear pET-32a was prepared by PCR using the primers, 5′-GTCGACAAGCTTGCGGCCGC-3′ (sense) and 5′-AGAACCGCGTGGCACCAGAC-3′ (antisense). Expression plasmids of AtBGlu42 mutants were prepared using a PrimeSTAR Mutagenesis Basal Kit (Takara Bio) with the following primers: for R342Y, 5′-TTGGAGTATATTGTTGAACTGGAAAAT-3′ (sense, substituted nucleotides underlined) and 5′-AACAATATACTCCAATTCTTGTGCTTG-3′ (antisense); and for R342A, 5′-TTGGAGGCGATTGTTGAACTGGAAAAT-3′ (sense) and 5′-AACAATCGCCTCCAATTCTTGTGCTTG-3′ (antisense). The DNA sequences encoding AtBGlu42 and neighboring regions were verified in all the expression constructs by DNA sequencing using an Applied Biosystems 3130 Genetic Analyzer (Thermo Fisher Scientific). The AtBGlu42-coding sequence was identical to the deposited cDNA sequence (Locus tag: AT5G36890.1).

Preparation of recombinant AtBGlu42

Recombinant AtBGlu42 was produced in *E. coli* as a fusion protein with thioredoxin and a His_6 tag at its N-terminus. *E. coli* Origami B(DE3) transformant, harboring the AtBGlu42 expression plasmid, was cultured in 1.0 L of Luria-Bertani medium containing 100 μg mL^{-1} ampicillin at 37 °C until the culture A_{600} reached 0.5. Recombinant protein production was induced by the addition of isopropyl β-D-1-thiogalactpyranoside (Wako Pure Chemical Industries) to be 0.1 mM in the medium and the incubation continued at 20 °C for 20 h with vigorous shaking. The *E. coli* cells were harvested

by centrifugation (7,000 × *g*, 4 °C, 10 min), and suspended in 30 mL of 20 mM sodium phosphate buffer (pH 7.5) containing 0.5 M NaCl (buffer A). The bacterial cells were disrupted by sonication using a Sonifier 450 (Branson, Danbury, CT, USA), and the supernatant was obtained by centrifugation (32,000 × *g*, 4 °C, 10 min). It was loaded onto a Ni immobilized Chelating Sepharose Fast Flow column (1.6 cm i.d. × 2.5 cm, 5 mL; GE Healthcare, Uppsala, Sweden), equilibrated with buffer A. After thoroughly washing the column with buffer A containing 30 mM imidazole, the adsorbed protein was eluted by a linear gradient of imidazole from 30 to 500 mM in buffer A (total elution volume, 200 mL). Fractions containing highly purified enzyme were pooled. Purity of the protein was confirmed by SDS-PAGE. The collected sample was dialyzed against 20 mM sodium phosphate buffer (pH 7.0) and concentrated to 2.49 mg mL^{-1} using an Amicon Ultra-15 centrifugal filter (30,000 nominal molecular weight limits; Merck Millipore, Billerica, MA, USA). The preparation was stored at 4 °C until use. The AtBGlu42 mutants were prepared in the same fashion as the wild type.

For X-ray crystallography, recombinant AtBGlu42 obtained as above, but from 4 L fermentation, was digested with thrombin (Sigma Aldrich, St. Louis, MO, USA) to remove its N-terminal region containing thioredoxin and a His_6 tag. Thrombin was added to the enzyme at a protein ratio of 1:20 (w/w) and it was incubated for 20 h at 4 °C. The untagged AtBGlu42 was collected in the non-adsorbed fractions in the Ni-affinity column chromatography done as described above, dialyzed against 20 mM Tris-HCl buffer (pH 7.2) (buffer B), and further purified by anion exchange column chromatography with a DEAE Sepharose Fast Flow column (2.5 cm i.d. × 16 cm, 78 mL; GE Healthcare) equilibrated with buffer B. After washing with buffer B, adsorbed protein was eluted with a linear gradient of NaCl from 0 to 0.5 M in buffer B (400 mL). The highly purified fractions were pooled, dialyzed against buffer B, and concentrated to 16.1 mg mL^{-1} as described above. The purified enzyme preparations were stored at 4 °C until use.

The protein concentration of the purified enzymes was determined based on the molar quantities of each amino acid measured using the ninhydrin colorimetric method with JLC-500/V (JEOL, Tokyo, Japan) after complete acid hydrolysis of the enzyme in 6 M HCl at 110 °C for 24 h.

Standard enzyme assay

Enzyme activity was measured using *p*-nitrophenyl β-D-glucopyranoside (pNP β-Glc, Sigma Aldrich) as substrate. A reaction mixture (50 μL), consisting of an appropriate concentration of enzyme, 50 mM sodium phosphate buffer (pH 6.8), 0.2 mg mL^{-1} bovine serum albumin (BSA), and 1 mM pNP β-Glc, was incubated at 30 °C for 10 min. The reaction was terminated by adding 25 μL of 2 M Na_2CO_3, and A_{400} was measured to determine the *p*-nitrophenol (pNP) with molar extinction coefficient of 18750 M^{-1} cm^{-1}. One unit (U) of β-glucosidase activity was defined as the amount of enzyme that releases 1 μmol of pNP in 1 min under these conditions.

Evaluation of effects of pH and temperature on activity and stability

Optimal pH was determined as the standard activity assay but using 80 mM modified Britton-Robinson buffer (pH 4.1-11.0; mixture of 80 mM sodium acetate, sodium phosphate, and glycine-NaOH buffers) in place of 50 mM sodium phosphate buffer. Optimum temperature was determined by measuring activities at 25-60 °C. The pH stability was determined based on residual activity after keeping 0.89 μM enzyme in 195 mM modified Britton-Robinson buffer (pH 4.1-11.2) at 4 °C for 24 h. Temperature stability was determined based on residual activity after keeping 24.2 nM enzyme in 12.5 mM sodium phosphate buffer (pH 7.0) containing 1 mg mL^{-1} BSA at 4-60 °C for 15 min. The ranges of pH and temperature in which the enzyme retained more than 90% of its original activity were defined the stable ranges.

Substrate specificity

Reaction rates to the following substrates (2 mM) were measured under the conditions of the standard enzyme assay: pNP β-Glc, pNP β-D-fucopyranoside (pNP β-D-Fuc), pNP β-D-galactopyranoside (pNP β-Gal), pNP β-D-mannopyranoside (pNP β-Man), pNP β-D-xylopyranoside (pNP β-Xyl), cellobiose, sophorose, pNP β-cellobioside, arbutin, phlorizin (Sigma Aldrich), cellotriose, cellotetraose, cellopentaose, cellohexaose, laminaribiose, laminaritriose, laminaritetraose

(Megazyme, Bray, Ireland), gentiobiose, methyl β-D-glucopyranoside (Nacalai Tesque, Kyoto, Japan), neotrehalose (Hayashibara, Okayama, Japan), 4-methylumbelliferyl β-D-glucopyranoside (4MU β-Glc), helicin, octyl β-D-glucopyranoside (Tokyo Chemical Industry, Tokyo, Japan), scopolin (Indofine Chemical Company, Hillsborough, NJ, USA), phenyl β-D-glucopyranoside (Kanto Chemical, Tokyo, Japan), and salicylic acid β-D-glucopyranoside (Grynkiewicz *et al.* 1993). pNP release rates from pNP glycosides, except pNP β-cellobioside, and D-glucose release rates from the others were measured. D-Glucose was quantified using the Glucose CII Test (Wako Pure Chemical Industries) after the enzyme reactions (50 μL) were terminated by the addition of 25 μL of 4 M Tris-HCl buffer (pH 7.0).

Kinetic parameters of the Michaelis-Menten equation were determined using non-linear regression in the s-*v* plots, in which substrate concentrations were as follows: 0.05-0.6 mM for pNP β-Glc; 0.05-0.8 mM for pNP β-D-Fuc, 4MU β-Glc, cellotriose, cellotetraose, cellopentaose, cellohexaose, laminaritriose, and laminaritetraose; 0.5-8 mM for pNP β-Gal; 0.1-1.6 mM for pNP β-Man; 0.125-2 mM for pNP β-Xyl, laminaribiose, and sophorose; 0.75-12 mM for cellobiose; 1-12 mM for gentiobiose; 0.0125-0.4 mM for pNP β-cellobioside and helicin; and 0.025-0.4 mM for scopolin. Fitting was done using Grafit version 7.0.2 (Erithacus Software, East Grinstead, UK). Subsite affinities for binding to cellooligosaccharides were calculated from the kinetic parameters according to the subsite theory for exo-glycosidase (Hiromi *et al.* 1973; Saburi *et al.* 2006).

Kinetic analysis of the reaction with pNP β-Glc

The reaction for pNP β-Glc was analyzed by nonlinear regression based on the kinetic model of retaining glycosidases that catalyze both hydrolysis and transglycosylation (Kobayashi *et al.* 2011; Saburi *et al.* 2013). Reaction equations used are as follows:

$$v_{ag} = v_h + v_{tg} \quad \text{(eq. 1)}$$

$$v_h = k_{cat1} K_{m2} s / (s^2 + K_{m2} s + K_{m1} K_{m2}) \quad \text{(eq. 2)}$$

$$v_{tg} = k_{cat2} s^2 / (s^2 + K_{m2} s + K_{m1} K_{m2}) \quad \text{(eq. 3)}$$

$$r_{tg} = v_{tg} / v_{ag} = s / (K_{TG} + s) \quad \text{(eq. 4)}$$

Here, s is pNP β-Glc concentration; v_{ag}, v_h, and v_{tg} are reaction rates of aglycone release, hydrolysis, and transglucosylation, respectively; r_{tg} is transglucosylation ratio, and K_{TG} is transglycosylation parameter. The kinetic parameters k_{cat1}, k_{cat2}, K_{m1}, and K_{m2} are defined as follows by the rate constants shown in Figure 1:

$$k_{cat1} = k_1k_2k_3(k_{-4} + k_5)/\{k_4k_5(k_{-1} + k_2) + k_1(k_{-4} + k_5)(k_2 + k_3)\}$$

$$k_{cat2} = k_2k_5/(k_2 + k_5)$$

$$K_{m1} = k_3(k_{-1} + k_2)(k_{-4} + k_5)/\{k_4k_5(k_{-1} + k_2) + k_1(k_{-4} + k_5)(k_2 + k_3)\}$$

$$K_{m2} = \{k_4k_5(k_{-1} + k_2) + k_1(k_{-4} + k_5)(k_2 + k_3)\}/\{k_1k_4(k_2 + k_5)\}$$

A reaction mixture (250 μL), containing 14.3 nM AtBGlu42, 50 mM sodium phosphate buffer (pH 6.8), 0.2 mg mL^{-1} BSA, and 0.125-8 mM pNP β-Glc, was incubated at 30 °C for 10 min. Aliquots (100 μL each) were taken, and the reaction was stopped with 200 μL of 1 M Na_2CO_3 and 50 μL of 4 M Tris-HCl buffer (pH 7.0) to measure pNP and D-glucose, respectively, as described above. The parameters, k_{cat1}, K_{m1}, and K_{m2}, were determined by nonlinear regression of equation 2 to the data. Then, k_{cat2} was determined from equations 1 and 3.

TLC analysis of reaction products from pNP β-Glc

A reaction mixture (200 μL), containing 2.27 μM AtBGlu42, 50 mM sodium phosphate buffer (pH 6.8), 0.2 mg mL^{-1} BSA, and 8 mM pNP β-Glc, was incubated at 30 °C for 30 min. Aliquots (10 μL) were taken at the indicated times and incubated at 100 °C for 2 min to terminate the reaction. TLC was done on Silica-gel (Aluminum TLC plate, Silica gel 60 F_{254}, Merck, Darmstadt, Germany) using a developing solvent chloroform/methanol/water (14/6/1; v/v/v). Spots of pNP glycosides were visualized by UV irradiation and carbohydrates were detected by spraying a detection reagent acetic acid/sulfuric acid/anisaldehyde (100/2/1; v/v/v) and heating.

Crystallization and data collection

Crystallization of the non-tagged AtBGlu42 was performed by the sitting-drop vapor diffusion method, in which 0.75 μL of protein solution (16.1 mg mL^{-1} in 20 mM Tris-HCl buffer, pH 7.2) was

mixed with an equal volume of reservoir solution containing 0.1 M sodium cacodylate buffer (pH 6.5), 0.2 M calcium acetate, and 18% (w/v) polyethylene glycol 8000 (Sigma Aldrich), and incubated at 20 °C for 2 months. X-ray diffraction data of AtBGlu42 were collected on the beam-line BL41XU at SPring-8 (Sayo, Japan). The data sets were indexed, integrated, scaled, and merged using the XDS program suite (Kabsch 2010). The asymmetric unit of AtBGlu42 contained one molecule corresponding to a Matthews coefficient (Matthews 1968) of 2.20 $Å^3\,Da^{-1}$ and an estimated solvent content of 44.2%. All the data collection statistics are summarized in **Table 1**.

Structure solution and refinement

The structure of AtBGlu42 was determined by the molecular replacement method with the program Phaser in the PHENIX program package (McCoy *et al.* 2007; Adams *et al.* 2010). The structure of Os3BGlu6 (52% sequence identity to AtBGlu42; PDB entry, 3GNO) (Seshadri *et al.* 2009) was used as the search model. Several rounds of refinement were performed using the program PHENIX.REFINE in the PHENIX program package, alternating with manual fitting and rebuilding based on $2F_o{-}F_c$ and $F_o{-}F_c$ electron densities in COOT (Emsley and Cowtan 2004). Water molecules and glycerol were built based on $2F_o{-}F_c$ and $F_o{-}F_c$ electron densities. The final refinement statistics and geometry defined by MOLPROBITY (Chen *et al.* 2010) are shown in **Table 1**. The atomic coordinates and structure factors were deposited in the Protein Data Bank (PDB entry, 7F3A). All structure figures were generated by PYMOL ver. 2.1 (Schrödinger, LLC, New York, NY, USA).

Molecular docking

Molecular docking was performed using AutoDock Vina (ADT version 1.5.6) (Trott and Olson 2010) to predict the interaction between AtBGlu42 and scopolin. Scopolin was prepared with the glucosyl moiety in the $^1S_3$ skew boat conformation with the Discovery Studio 4.0 program (Dassault Systèmes BIOVIA, San Diego, CA, USA). Water molecules and glycerol molecules in the active site of AtBGlu42 were removed for the docking test. The scopolin was docked into the active site of

AtBGlu42 using the grid box with a spacing of 1 Å and dimension of 40×40×40, centered at positions of 15.80 (x), 63.04 (y), 43.12 (z). The exhaustiveness value was set to 8.

Results

Preparation of recombinant AtBGlu42

A cDNA prepared from *A. thaliana* seedling RNA was used to produce AtBGlu42 in recombinant *E. coli* as a fusion protein with a 131-residue-long vector-derived region containing thioredoxin and a His_6 tag on the N-terminal side of Met1 of AtBGlu42. From the cell-free extract obtained from 1 L of culture, 8.8 mg of the recombinant enzyme was purified by immobilized metal (Ni) affinity column chromatography. The molecular mass of recombinant AtBGlu42, estimated by SDS-PAGE, was 70 kDa, and it coincided with the theorical mass from the amino acid sequence (70,143 Da) (**Figure 2**). Its specific activity was 10.5 U mg^{-1}. The optimum pH and temperature were pH 6.8 and 40 °C, respectively (**Figure 3a and b**). AtBGlu42 retained over 90% of the original activity after incubation at pH 6.3-9.3 at 4 °C for 24 h, or up to 35 °C at pH 7.0 for 15 min (**Figure 3c and d**).

Specificity to pNP β-glycosides

The glycone specificity of AtBGlu42 was evaluated based on the reaction velocities to 2 mM pNP β-glycosides and kinetic parameters (**Table 2**). pNP β-Glc and pNP β-D-Fuc were good substrates, but AtBGlu42 acted also on β-galactoside, β-mannoside, and β-xyloside with lower velocities. AtBGlu42 catalyzed transglucosylation for pNP β-Glc. In the early stage of the reaction with 8 mM pNP β-Glc, transglucosylation products, including pNP β-cellobioside, were observed in the TLC analysis, and the substrate and transglucosylation products were completely hydrolyzed within 30 min of reaction (**Figure 4a and b**). Velocities for aglycone release (v_{ag}), hydrolysis (v_h), and transglucosylation (v_{tg}) were calculated from velocities for the liberation of pNP and D-glucose (**Figure 4c**). These reaction velocities followed the rate equations 1-3 of a retaining glycoside hydrolase catalyzing both hydrolysis and transglucosylation simultaneously with kinetic parameters as

follows: k_{cat1}, 9.15 ± 0.08 s^{-1}, k_{cat2}, 37.8 ± 1.2 s^{-1}, K_{m1}, 0.127 ± 0.002 mM, and K_{m2}, 26.1 ± 0.7 mM (**Figure 4c**). The kinetic parameter k_{cat1}/K_{m1}, which is comparable to k_{cat}/K_m of the Michaelis-Menten equation, was 71.9 s^{-1} mM^{-1}. The transglucosylation ratio, $r_{tg} = v_{tg} / v_{ag}$, followed the equation 4 with K_{TG} of 6.30 ± 0.08 mM, at which $v_h = v_{tg}$ is obtained (**Figure 4d**). In the lower pNP β-Glc concentrations (≤ 0.6 mM), the reaction velocity for aglycone release followed Michaelis-Menten equation with k_{cat}/K_m (72.2 s^{-1} mM^{-1}), which was consistent with k_{cat1}/K_{m1}. Compared with k_{cat1}/K_{m1} of pNP β-Glc, k_{cat}/K_m of pNP β-D-Fuc, 81.3 s^{-1} mM^{-1}, was similar, but those of pNP β-Gal, pNP β-Man, and pNP β-Xyl were only 1.9%, 1.1%, and 0.40% that of pNP β-Glc, respectively (**Table 2**).

Specificity to various β-glucosides

Reaction velocity was measured with 2 mM of various β-glucosides (**Table 2**). Reaction velocities towards helicin, 4MU β-Glc, and scopolin were high, but those towards phenyl β-glucoside, arbutin, salicylic acid β-glucoside, phlorizin, methyl β-glucoside, and octyl β-glucoside were low or undetectable. k_{cat}/K_m for helicin, 160 s^{-1} mM^{-1}, was the highest of the tested substrates, followed by those of scopolin (104 s^{-1} mM^{-1}) and 4MU β-Glc (97 s^{-1} mM^{-1}). Thus, the scopolin hydrolytic activity of AtBGlu42, predicted in the plant reverse genetics studies (Zamioudis, Hanson and Pieterse 2014; Stringlis *et al.* 2018), was enzymatically confirmed.

Specificity to β-glucooligosaccharides

AtBGlu42 hydrolyzed various β-glucobioses (**Table 2**). Among the disaccharides, laminaribiose (Glcβ1-3Glc) was the best substrate in terms of k_{cat}/K_m, 94.6 s^{-1} mM^{-1}, followed by sophorose (Glcβ1-2Glc, 13.8 s^{-1} mM^{-1}). Those of cellobiose (Glcβ1-4Glc), gentiobiose (Glcβ1-6Glc), and neotrehalose (Glcβ1-α1Glc) were very low or undetectable. The highest k_{cat}/K_m was for laminaribiose of laminarioligosaccharides, but for cellotriose (85.5 s^{-1} mM^{-1}) of cellooligosaccharides. The decrease in k_{cat}/K_m values with increasing degree of polymerization above that of the best substrates was milder with cellooligosaccharides than with laminarioligosaccharides.

Structural analysis

For the crystal structure analysis, the N-terminal tag of the recombinant AtBGlu42 was removed by cleavage with thrombin and column chromatographies. The untagged protein possesses two extra residues, Gly-Ser, before Met1 of the registered sequence. The specific activity of the untagged enzyme (56.2 kDa) was 16.9 ± 0.3 U mg^{-1}, corresponding to 15.8 ± 0.3 s^{-1}, which is close to that of the recombinant enzyme without removal of the N-terminal region. The structure of the untagged AtBGlu42 was determined at 1.7 Å resolution by X-ray crystallography (**Table 1**). Because of poor electron density, the N-terminal Gly, nine C-terminal residues Asp482–Glu490, and a part of β→α loop 6 Lys328–Glu331 were not built. The overall structure of AtBGlu42 was a $(\beta/\alpha)_8$-barrel, as are all known GH1 enzyme structures (**Figure 5a**). An extra N-terminal α-helix was located suitably to interact with the small domain composed of β→α loops 5 and 6, in which a three-stranded β-sheet consisting of β5′, β6′, and β6″ was observed. This extra α-helix was not found in the other GH1 structures, and the other *A. thaliana* and rice GH1 homologues, including Os1BGlu4, do not have the amino acid sequence corresponding to the extra α-helix. The putative catalytic residues of AtBGlu42 (Glu183 and Glu388 on β-strands 4 and 7, respectively) and the residues interacting with the glucose moiety in subsite −1 (Gln35, His137, Asn182, Tyr317, Glu388, Trp437, Glu444, Trp445, and Phe453) are positioned similarly to those of known GH1 β-glucosidase structures (**Figure 6a**). Electron density for four molecules of glycerol used as a cryoprotectant was observed. Two glycerol molecules were located on the β→α loop 1 (**Figure 5a**). The other two were located in subsites −1 and +1 with possible hydrogen bonds with Gln35, His137, Asn182, Glu183, Glu388, Glu444, and Trp445 (**Figure 5b**). The glycerol in subsite −1 was placed in the position corresponding to 2-C to 4-C of the substrate analogous inhibitors (glucoimidazole and 1-deoxynojirimycin) bound to subsite −1 in other GH1 β-glucosidases: Os3BGlu7 (PDB entry, 7BZM) (Nutho *et al.* 2020) and Tmari_1862 (PDB entry, 2CES) (Gloster *et al.* 2006) (**Figure 6a**). Three O atoms of the glycerol were at the same positions of 2-O and 3-O of the inhibitors, but not at that of 4-O.

We compared the structures of AtBGlu42 with the Os3BGlu7 (Chuenchor *et al.* 2011) to explore the structure involved in binding of laminaribiose and cellooligosaccharides. The acid/base

catalyst Glu183 of AtBGlu42 is at the same position as Glu176 (Gln in the structure) of Os3BGlu7-laminaribiose complex to form hydrogen bonds with 2-O and 3-O (glucosidic oxygen) of the glucose moiety at subsite +1, but Glu246 equivalent to Asn245 of Os3BGlu7 is far from 1-O. Instead, Asp244 is suitably located to form a hydrogen bond with 1-O, while corresponding Asp243 of Os3BGlu7 is differently oriented toward Arg178 **(Figure 6b and c**). In the Os3BGlu7-cellopentaose complex, three residues, Asn245 on β→α loop 5, Tyr341 and Trp358 on β→α loop 6, are placed to interact with cellopentaose in subsites +1 to +4 **(Figure 6d**). The corresponding residues in AtBGlu42, Glu246, Arg342, and Trp360, are placed in the equivalent positions. The Glu246 side chain, differently oriented from Asn245 of Os3BGlu7, is also in a good position to form subsite +2 and no obvious steric hindrance at subsite +1 and +2 is observed, but the side chain of Arg342 seems to occupy the space for subsite +3 to cause a steric hindrance upon binding to cellooligosaccharide in subsite +3 **(Figure 6e**). The distance between Arg342 and the glucosyl residue at subsite +3 is too short (1.7 Å between Arg342 Nη1 and Glc 5-C; 2.5 Å between Arg342 Nη2 and Glc 6-C).

Analysis of Arg342 mutants

The role of Arg342 in cellooligosaccharide selection was investigated through analysis of the activity of Arg342 mutants, R342A and R342Y, on cellooligosaccharide (**Table 3**). The k_{cat}/K_m values of R342A and R342Y for cellobiose were 72% and 5.4% of that of the wild type, respectively. Those for pNP β-Glc were 52% and 6.9% of the wild type, respectively. Greater reductions in R342Y than in R342A were observed for all the tested cellooligosaccharides, mainly because of this decrease in k_{cat}. The values of k_{cat} in R342Y for pNP β-Glc and cellooligosaccharides decreased to 12-14% of those of the wild type with unknown reason. The cellotriose preference of the wild type was not observed in the mutants. The highest k_{cat}/K_m of R342A and R342Y was to cellopentaose and cellotetraose, respectively. The ratio of k_{cat}/K_m of cellotetraose over cellotriose was 0.52 in the wild type, but 1.2 and 2.7 in R342A and R342Y, respectively. Subsite affinities were calculated (**Table 4**). Affinity of subsite +3 was negative in the wild type (−1.64 kJ mol^{-1}), but positive affinity (0.470 kJ mol^{-1} and 2.54 kJ

354 mol^{-1}, respectively) was obtained in R342A and R342Y. The negative affinity observed at subsite +4
355 in the wild type was also changed to favorable or less unfavorable by the Arg342 mutations.
356
357 **Docking simulation of AtBGlu42 and scopolin**
358 Binding mode of scopolin in AtBGlu42 was predicted by docking simulation using AutoDock
359 Vina. The binding energy of water-free AtBGlu42 and scopolin was calculated to be −37.2 kJ mol^{-1}.
360 In the obtained structure, the glucosyl residue of scopolin was accommodated in subsite −1, as
361 observed in other GH1 complex structures, with possible interactions to Gln35, His137, Asn182,
362 Tyr317, Glu388, Trp437, Glu444, Trp445, and Phe453 (**Figure 7**). The umbelliferyl plane of the
363 aglycone part was placed to face Trp360 for the possible stacking interaction. The 6-methoxy group of
364 scopolin was at a distance from Phe197 (3.8 Å between C–C, 3.4 Å between C–O).
365
366 **Discussion**
367 Plants possess numerous GH1 β-glucosidase isoenzymes, and they are involved in various
368 biological processes including development and biotic/abiotic stress responses. The functional
369 characterization of the enzymes is important to address their physiological functions and
370 understanding the molecular basis of the enzymatic functions makes it possible to predict enzyme
371 function more accurately. AtBGlu42, a putative cytosolic GH1 β-glucosidase, was previously
372 implicated, by the reverse genetic approach, to be responsible for the hydrolysis of scopolin in roots to
373 release an iron-chelating agent scopoletin into the rhizosphere under iron-deficient conditions
374 (Zamioudis, Hanson and Pieterse 2014; Stringlis *et al.* 2018). This suggests that AtBGlu42 is highly
375 specific to this β-glucoside, but the homologous enzyme Os1BGlu4 from rice plant efficiently
376 catalyzes the hydrolysis of cello- and laminari-oligosaccharides in addition to the β-glucosides of
377 plant secondary metabolites (Rouyi *et al.* 2014). In this study, the activity of AtBGlu42 on scopolin
378 and various substrates, including these oligosaccharides, was clarified along with the associated
379 protein structure using the enzyme produced by recombinant expression.

Recombinant AtBGlu42 was the most active at a neutral pH, similar to Os1BGlu4 (Rouyi *et al.* 2014). This optimum pH is suitable for the action in the cytoplasm since its pH in plants is neutral (Shen *et al.* 2013). The homologous rice protein Os1BGlu4 possesses no signal peptide in its precursor sequence, and its cytoplasmic localization has been demonstrated in maize protoplasts by transient expression of the Os1BGlu4-GFP fusion protein (Rouyi *et al.* 2014). AtBGlu42 is also presumably located in cytoplasm. In addition to the neutral pH optima, the substrate specificity of AtBGlu42 on those secondary metabolite glucosides and the short-chain oligosaccharides may be reasonable as a cytosolic enzyme.

The hydrolytic activity of AtBGlu42 on scopolin was confirmed in this study. AtBGlu42 hydrolyzed scopolin with the second highest k_{cat}/K_m of the tested substrates (**Table 2**). The docking simulation of AtBGlu42 and scopolin predicted van der Waals interaction of Phe197 with the 6-methoxy group and the stacking interaction of Trp360 with the umbelliferyl moiety, respectively (**Figure 7**). AtBGlu42 acted on 4MU β-Glc with almost the same k_{cat} and K_m as on scopolin, suggesting that the interaction of Phe197 with the 6-methoxy group of scopolin is comparable to the interaction between Trp360 and the 4-methyl group, which is expected to be formed assuming that the umbelliferyl ring of 4MU β-Glc binds in the same way as predicted for scopolin. The k_{cat}/K_m value of AtBGlu42 was 61-fold or much higher than those of other Arabidopsis GH1 β-glucosidase isoenzymes, AtBGlu21, AtBGlu22, and AtBGlu23, which are enzymes known to hydrolyze scopolin (Ahn *et al.* 2010). These isoenzymes have Lys and Ala residues at the position corresponding to Phe197 and Trp360 in AtBGlu42, respectively. Thus, Phe197 and Trp360 are presumably key residues for high activity to scopolin. Of the 40 Arabidopsis GH1 isoenzymes, three (AtBGlu44, AtBGlu45, and AtBGlu46) have a set of Phe and Trp residues in addition to AtBGlu42, and 12 of the 40 isoenzymes have Trp residue, which is thought to be important for stacking with the δ-lactone ring. Since many GH1 enzymes are highly active for 4MU β-Glc, and Trp residues are conserved in more than 80% of the approximately 300 characterized GH1 enzymes (mainly from bacteria), many GH1 enzymes may also act on scopolin efficiently.

406 Among the tested β-glucosides, AtBGlu42 showed the highest k_{cat}/K_m to helicin (2-*O*-
407 glucosylbenzaldehyde), higher than scopolin, and considerable activity to pNP β-Glc. On the other
408 hand, activity on phenyl β-glucoside, arbutin (*p*-hydroxyphenyl β-glucoside), salicylic acid β-
409 glucoside (2-*O*-glucosylbenzoic acid) and phlorizin were very low or undetectable (**Table 2**). The
410 aldehyde group of helicin could be equivalent to 6-methoxy group of scopolin, the carbon of which
411 was in a distance for hydrophobic interaction with Phe197 in the modelled complex structure (**Figure**
412 **7**). GH1 β-glucosidase from *Agrobacterium tumefaciens*, SghA, acts on salicylic acid β-glucoside
413 through the formation of hydrogen bonds between the carboxy group and His193, corresponding to
414 Phe197 of AtBGlu42 (Wang *et al.* 2019). Charged groups or groups bulkier than the aldehyde group
415 on this position of the phenyl group may not be accepted because of unfavorable interactions with
416 Phe197.
417 AtBGlu42 showed activity not only on β-glucosides but also on other β-glycosides (**Table 2**).
418 Among the tested pNP β-glycosides, pNP β-Glc and pNP β-D-Fuc (6-deoxy-D-galactoside) were good
419 substrates as observed in several plant β-glucosidases (Ketudat Cairns and Esen 2010). The much
420 lower k_{cat}/K_m values to pNP β-Gal and pNP β-Xyl were mainly due to high K_m values. pNP β-Man was
421 also a poor substrate but mainly due to low k_{cat}. This indicates that pNP β-Man is not favorable for the
422 formation of the transition state from the Michaelis complex. The axial 2-OH group of β-mannoside is
423 probably not suitable for the stabilization of the transition state in the active site of AtBGlu42.
424 Efficient activity on β-mannosides requires the ability to bind their transition state in the $B_{2,5}$ boat
425 conformation favored for mannoside hydrolysis rather than the $^4H_3$ half-chair or ^4E envelope-like
426 transition state of glucosides (Tankrathok *et al.* 2015). Subtle differences in the active site amino acid
427 residue positions apparently enable this in some GH1 enzymes, but not others, including AtBGlu42.
428 In the reaction with pNP β-Glc, AtBGlu42 catalyzed both hydrolysis and transglucosylation
429 with K_{TG} of 6.3 mM. The reaction rates for hydrolysis, transglucosylation, and aglycone release
430 obeyed well the reaction equations obtained based on the reaction scheme for retaining glycosidase
431 well. The transglucosylation products including pNP β-cellobioside were observed, as observed for
432 Os1BGlu4 (Rouyi *et al.* 2014), Os3BGlu7 (Opassiri *et al*. 2004), and HvBII (Hrmova *et al*. 1998).

The transglycosylation was not observed with the other pNP β-glycosides under the reaction conditions, suggesting that only β-glucoside can be bound in the suitable position for transglucosylation even though it must take a few binding modes to produce the transglycosylation products.

AtBGlu42 also hydrolyzed various β-glucooligosaccharides. In terms of k_{cat}/K_m, laminaribiose was the best substrate among the tested disaccharides and also among laminarioligosaccharides, while cellotriose was the best of cellooligosaccharides. The disaccharide preference among laminarioligosaccharides is often observed in plant β-glucosidases (Opassiri *et al.* 2004; Seshadri *et al.* 2009; Opassiri *et al.* 2010; Rouyi *et al.* 2014). The crystal structure of the Os3BGlu7-laminaribiose complex indicates that the reducing-terminal β-glucosyl residue of laminaribiose binds to subsite +1 in a similar position to the corresponding glucosyl unit of cellooligosaccharide, but the faces of their glucosyl units toward Trp358 were opposite to each other. Therefore 1-O of the laminaribiose is placed on the bottom of the cleft, close to 6-O of the Glc moiety in the cellooligosaccharide, with a possible hydrogen bond to Asn245 (Chuenchor *et al.* 2011) (**Figure 6b and d**). AtBGlu42 seems to possess the residues to accommodate laminaribiose at the similar position in the protein structure (**Figure 6c**). In the binding of longer laminarioligosaccharides, the corresponding Glc moiety needs to take another unfavorable binding mode in subsite +1 to avoid the steric hindrance. This could explain the disaccharide preference of laminarioligosaccharides **(Table 2)**.

The cellotriose preference of AtBGlu42 is caused by the negative affinity in subsite +3, mainly due to the steric hindrance with the Arg342 side chain. Structural comparison with the Os3BGlu7-cellopentaose complex clearly shows that the Arg342 side chain occupies the substrate binding cleft to cause steric hindrance in subsite +3 upon binding to cellooligosaccharides, while the corresponding Tyr341 in Os3BGlu7 has stacking interaction onto the glucosyl residue in subsite +3 (**Figure 6d and e**). The role of the Arg342 was supported by the results of its mutants, R342A and R342Y, both of which showed clear increases in the affinity in subsite +3 (**Table 4**). Particularly the affinity of R342Y (2.5 kJ mol^{-1}) is similar to that of Os3BGlu7 (2.2 kJ mol^{-1}) (Opassiri *et al.* 2004), implying that the Tyr substitution sets the binding site as in Os3BGlu7.

Arg342 is responsible for the cellotriose preference in AtBGlu42, but careful consideration is required to predict the cellooligosaccharide preference of other GH1 β-glucosidases, because some enzymes possessing Arg residues in the position do not exhibit a cellotriose preference. The homologous rice enzyme, Os1BGlu4, possesses equivalent Arg334, but exhibits the highest preference for cellotetraose of cellooligosaccharides with 1.9-fold higher k_{cat}/K_m than cellotriose (Rouyi *et al.* 2014). Its three-dimensional structure is not known yet, but the lack of the trisaccharide preference is possibly caused by a different orientation of the Arg334 side chain. One possible reason for it is interaction of Arg334 with its neighboring Glu336, corresponding to Val344 in AtBGlu42. Another example is a metagenomic β-glucosidase Td2F2. This enzyme, with 41% sequence identity with AtBGlu42, possesses the corresponding Arg313 (Matsuzawa *et al.* 2016), but it shows 1.5-fold higher k_{cat}/K_m to cellotetraose than to cellotriose (Uchiyama, Miyazaki and Yaoi 2013). The structural comparison revealed that the Arg residues in the both structures are placed in the same position in the local small domain structure composed of β→α loops 5 and 6, which contain β5′–α5′ and β6′–β6″, respectively. The three strands β5′, β6′, and β6″ comprise β-sheet in the small domain as in other GH1 enzymes, and the Arg residues are similarly located on β6″ in a three-stranded β-sheet (**Figure 8a and b**) (Matsuzawa *et al.* 2016). However, the Arg side chains in AtBGlu42 and Td2F2 are placed differently. One reason is different interactions with surrounding residues (**Figure 8a and b**). Arg342 of AtBGlu42 is in the position to form a salt bridge with Glu246 on β→α loop 5 (**Figure 8a**). In the Td2F2 structure, the corresponding residue is Thr225, and Arg313 has another interaction with the carbonyl oxygen of Arg297 in the N-terminal stretch of β6′, to place the side chain of Arg313 out of the glucosyl binding site (**Figure 8b**). The other reason is a shift of the small local domain location in the $(\beta/\alpha)_8$-barrel structure. The small domains are placed a bit differently while the β5, α5, β6, and α6 composing the $(\beta/\alpha)_8$-barrel are strictly placed in the same positions (**Figure 8c**). The small domain of AtBGlu42 is located closer to α6, compared with that of Td2F2. The distance between Cα atoms of Pro255 and Pro234, located at the N-terminus of α5′ of AtBGlu42 and Td2F2, respectively, is 7.0 Å in the superimposed structures. That of the Arg residues is 2.9 Å. The different placement of the local domains is stabilized by the interaction with the surrounding structures (**Figure 8d and e**). In the

Td2F2 structure, two salt bridges connecting α5′ to α6, and α5 to an α-helix adjacent to α5′ are observed (Asp244–Arg338 and Arg249–Asp263, respectively). In the structure of AtBGlu42, those salt bridges are not found, but a hydrophobic core, consisting of Trp247, Ile265, Lys370, and Tyr374, is formed between the small domain and α6. Mainly because of these differences, the small domains in the shifted positions each other are stabilized, providing the different surrounding circumstances to the Arg side chains.

In this study, we have elucidated the biochemical functions and structure of AtBGlu42, responsible to hydrolyze scopolin in Arabidopsis. Recombinant AtBGlu42 showed high activities not only toward scopolin, but also towards other β-glucosides such as helicin, laminaribiose, and cellotriose. The preference for chain-length of cellooligosaccharides was understood by possible steric hindrance caused by Arg342 on the β→α loop 6 at subsite +3. Combining the mutational study of AtBGlu42, we postulate β→α loop 6, including amino acid residue corresponding to Arg342 of AtBGlu42, is the key determinant of specificity to cellooligosaccharide chain-length in GH1 enzymes. Furthermore, structural comparison of GH1 β-glucosidases suggests that a mechanism for diversification of substrate binding site through variation in structures that do not directly interact with the substrates.

Acknowledgements

We thank Mr. Yusuke Takada of the DNA sequencing facility of the Research Faculty of Agriculture, Hokkaido University for assistance with DNA sequence analysis; and Ms. Nozomi Takeda of the Global Facility Center, Hokkaido University for the amino acid analysis. X-ray diffraction experiments were conducted at SPring-8 (proposals 2021A2756). We thank the beamline staff of SPring-8 for their assistance.

Data availability

The data underlying this article are available in the article.

Author contributions

S.H. conceived and designed the experiments, performed the biochemical experiments, determined the protein structure, and wrote the paper. W.S. conceived and designed the experiments, determined the protein structure, and wrote the paper. J.Y. determined the protein structure and wrote the paper. H.Matsuura prepared the substrate and wrote the paper. J.R.K.C. wrote the paper. M.Y. determined the protein structure and wrote the paper. H.Mori conceived and designed the experiments and wrote the paper.

Funding

This research was supported by Platform Project for Supporting Drug Discovery and Life Science Research (Basis for Supporting Innovative Drug Discovery and Life Science Research; BINDS) from AMED under grant no. JP18am00101071 and JP19am0101093.

Disclosure statement

No potential conflict of interest was reported by the authors.

References

Adams PD, Afonine PV, Bunkóczi G *et al*. *PHENIX*: a comprehensive Python-based system for macromolecular structure solution. *Acta Crystallogr D Biol Crystallogr* 2010;**66**:213-221.

Ahn YO, Shimizu B, Sakata K *et al*. Scopolin-hydrolyzing β-glucosidases in roots of Arabidopsis. *Plant Cell Physiol* 2010;**51**:132-143.

Baba SA, Vishwakarma RA, Ashraf N. Functional characterization of *Cs*BGlu12, a β-glucosidase from *Crocus sativus*, provides insights into its role in abiotic stress through accumulation of antioxidant flavonols. *J Biol Chem* 2017;**292**:4700-4713.

Babcock GD, Esen A. Substrate specificity of maize β-glucosidase. *Plant Sci* 1994;**101**:31-39.

Barleben L, Panjikar S, Ruppert M *et al*. Molecular architecture of strictosidine glucosidase: the gateway to the biosynthesis of the monoterpenoid indole alkaloid family. *Plant Cell* 2007;**19**:2886-2897.

Chen VB, Arendall WB III, Headd JJ *et al*. *MolProbity*: all-atom structure validation for macromolecular crystallography. *Acta Crystallogr D Biol Crystallogr* 2010;**66**:12-21.

Chuenchor W, Pengthaisong S, Robinson RC *et al*. The structural basis of oligosaccharide binding by rice BGlu1 beta-glucosidase. *J Struct Biol* 2011;**173**:169-179.

Emsley P, Cowtan K. *Coot*: model-building tools for molecular graphics. *Acta Crystallogr D Biol Crystallogr* 2004;**60**:2126-2132.

Gloster TM, Roberts S, Perugino G *et al*. Structural, kinetic, and thermodynamic analysis of glucoimidazole-derived glycosidase inhibitors. *Biochemistry* 2006;**45**:11879-11884.

Grynkiewicz G, Achmatowicz O, Hennig J *et al.* Synthesis and characterization of the salicylic acid β-D-glucopyranoside. *Pol J Chem* 1993;**67**:1251-1254.

Henrissat B, Callebaut I, Fabrega S *et al*. Conserved catalytic machinery and the prediction of a common fold for several families of glycosyl hydrolases. *Proc Natl Acad Sci USA* 1995;**92**:7090-7094.

Himeno N, Saburi W, Wakuta S *et al*. Identification of rice β-glucosidase with high hydrolytic activity towards salicylic acid β-D-glucoside. *Biosci Biotechnol Biochem* 2013;**77**:934-939.

Hiromi K, Nitta Y, Numata C *et al.* Subsite affinities of glucoamylase: examination of the validity of the subsite theory. *Biochim Biophys Acta* 1973;**302**:362-375.

Hösel W, Tober I, Eklund SH *et al*. Characterization of β-glucosidases with high specificity for the cyanogenic glucoside dhurrin in *Sorghum bicolor* (L.) Moench seedlings. *Arch Biochem Biophys* 1987;**252**:152-162.

Hrmova M, MacGregor EA, Biely P *et al*. Substrate binding and catalytic mechanism of a barley β-D-Glucosidase/(1,4)-β-D-glucan exohydrolase. *J Biol Chem* 1998;**273**:11134-11143.

Hua Y, Sansenya S, Saetang C *et al*. Enzymatic and structural characterization of hydrolysis of gibberellin A4 glucosyl ester by a rice β-D-glucosidase. *Arch Biochem Biophys* 2013;**537**:39-48.

Jenkins J, Lo Leggio L, Harris G *et al*. β-Glucosidase, β-galactosidase, family A cellulases, family F xylanases and two barley glycanases form a superfamily of enzymes with 8-fold β/α

architecture and with two conserved glutamates near the carboxy-terminal ends of β-strands four and seven. *FEBS Lett* 1995;**362**:281-285.

Kabsch W. *XDS*. *Acta Crystallogr D Biol Crystallogr* 2010;**66**:125-132.

Ketudat Cairns JR, Esen A. β-Glucosidases. *Cell Mol Life Sci* 2010;**67**:3389-3405.

Ketudat Cairns JR, Pengthaisong S, Luang S *et al.* Protein-carbohydrate interactions leading to hydrolysis and transglycosylation in plant glycoside hydrolase family 1 enzymes. *J Appl Glycosci* 2012;**59**:51-62.

Ketudat Cairns JR, Mahong B, Baiya S *et al*. β-Glucosidases: Multitasking, moonlighting or simply misunderstood? *Plant Sci* 2015;**241**:246-259.

Kobayashi M, Hondoh H, Mori H *et al*. Calcium ion-dependent increase in thermostability of dextran glucosidase from *Streptococcus mutans*. *Biosci Biotechnol Biochem* 2011;**75**:1557-1563.

Lee KH, Piao HL, Kim HY *et al*. Activation of glucosidase via stress-induced polymerization rapidly increases active pools of abscisic acid. *Cell* 2006;**126**:1109-1120.

Lombard V, Golaconda Ramulu H, Drula E *et al.* The carbohydrate-active enzymes database (CAZy) in 2013. *Nucleic Acids Res* 2014;**42**:D490-495.

McCoy AJ, Grosse-Kunstleve RW, Adams PD *et al*. *Phaser* crystallographic software. *J Appl Crystallogr* 2007;**40**:658-674.

Matsuzawa T, Jo T, Uchiyama T *et al*. Crystal structure and identification of a key amino acid for glucose tolerance, substrate specificity, and transglycosylation activity of metagenomic β-glucosidase Td2F2. *FEBS J* 2016;**283**:2340-2353.

Matthews BW. Solvent content of protein crystals. *J Mol Biol* 1968;**33**:491-497.

Nutho B, Pengthaisong S, Tankrathok A *et al*. Structural basis of specific glucoimidazole and mannoimidazole binding by Os3BGlu7. *Biomolecules* 2020;**10**:907.

Opassiri R, Hua Y, Wara-Aswapati O *et al*. β-Glucosidase, exo-β-glucanase and pyridoxine transglucosylase activities of rice BGlu1. *Biochem J* 2004;**379**:125-131.

Opassiri R, Pomthong B, Onkoksoong T *et al*. Analysis of rice glycosyl hydrolase family 1 and expression of Os4bglu12 β-glucosidase. *BMC Plant Biol* 2006;**6**:33.

596 Opassiri R, Maneesan J, Akiyama T *et al*. Rice Os4BGlu12 is a wound-induced β-glucosidase that
597 hydrolyzes cell wall-β-glucan-derived oligosaccharides and glycosides. *Plant Sci*
598 2010;**179**:273-280.
599 Roepke J, Bozzo GG. *Arabidopsis thaliana* β-glucosidase BGLU15 attacks flavonol 3-*O*-β-glucoside-
600 7-*O*-α-rhamnosides. *Phytochemistry* 2015;**109**:14-24.
601 Rouyi C, Baiya S, Lee SK *et al*. Recombinant expression and characterization of the cytoplasmic rice
602 β-glucosidase Os1BGlu4. *PLoS One* 2014;**9**:e96712.
603 Rye CS, Withers SG. Glycosidase mechanisms. *Curr Opin Chem Biol* 2000;**4**:573-580.
604 Saburi W, Mori H, Saito S *et al.* Structural elements in dextran glucosidase responsible for high
605 specificity to long chain substrate. *Biochim Biophys Acta* 2006;**1764**:688-698.
606 Saburi W, Kobayashi M, Mori H *et al.* Replacement of the catalytic nucleophile aspartyl residue of
607 dextran glucosidase by cysteine sulfinate enhances transglycosylation activity. *J Biol Chem*
608 2013;**288**:31670-31677.
609 Seshadri S, Akiyama T, Opassiri R *et al.* Structural and enzymatic characterization of Os3BGlu6, a
610 rice β-glucosidase hydrolyzing hydrophobic glycosides and (1→3)- and (1→2)-linked
611 disaccharides. *Plant Physiol* 2009;**151**:47-58.
612 Shen J, Zeng Y, Zhuang X *et al*. Organelle pH in the *Arabidopsis* endomembrane system. *Mol Plant*
613 2013;**6**:1419-1437.
614 Stringlis IA, Yu K, Feussner K *et al*. MYB72-dependent coumarin exudation shapes root microbiome
615 assembly to promote plant health. *Proc Natl Acad Sci USA* 2018;**115**:E5213-5222.
616 Sue M, Ishihara A, Iwamura H. Purification and characterization of a hydroxamic acid glucoside β-
617 glucosidase from wheat (*Triticum aestivum* L.) seedlings. *Planta* 2000;**210**:432-438.
618 Tankrathok A, Iglesias-Fernández J, Williams RJ *et al*. A single glycosidase harnesses different
619 pyranoside ring transition state conformations for hydrolysis of mannosides and glucosides.
620 *ACS Catal* 2015;**5**:6041-6051.
621 Trott O, Olson AJ. AutoDock Vina: improving the speed and accuracy of docking with a new scoring
622 function, efficient optimization, and multithreading. *J Comput Chem* 2010;**31**:455-461.

623 Uchiyama T, Miyazaki K, Yaoi K. Characterization of a novel β-glucosidase from a compost
624 microbial metagenome with strong transglycosylation activity. *J Biol Chem* 2013;**288**:18325-
625 18334.
626 Wakuta S, Hamada S, Ito H *et al*. Identification of a β-glucosidase hydrolyzing tuberonic acid
627 glucoside in rice (*Oryza sativa* L.). *Phytochemistry* 2010;**71**:1280-1288.
628 Wakuta S, Hamada S, Ito H *et al.* Comparison of enzymatic properties and gene expression profiles of
629 two tuberonic acid glucoside β-glucosidases from *Oryza sativa* L. *J Appl Glycosci*
630 2011;**58**:67-70
631 Wang C, Ye F, Chang C *et al.* Agrobacteria reprogram virulence gene expression by controlled
632 release of host-conjugated signals. *Proc Natl Acad Sci USA* 2019;**116**:22331-22340.
633 Xia L, Ruppert M, Wang M *et al*. Structures of alkaloid biosynthetic glucosidases decode substrate
634 specificity. *ACS Chem Biol* 2012;**7**:226-234.
635 Xu Z, Escamilla-Treviño LL, Zeng L *et al*. Functional genomic analysis of *Arabidopsis thaliana*
636 glycoside hydrolase family 1. *Plant Mol Biol* 2004;**55**:343-367.
637 Zamioudis C, Hanson J, Pieterse CMJ. β-Glucosidase BGLU42 is a MYB72-dependent key regulator
638 of rhizobacteria-induced systemic resistance and modulates iron deficiency responses in
639 *Arabidopsis* roots. *New Phytol* 2014;**204**:368-379.
640
641 **Figure captions**
642 **Graphical abstract**
643 The cellotriose specificity of AtBGlu42 was attributed to R342, and the chain length specificity was
644 modified by mutation of R342.
645
646 **Figure 1.** Reaction scheme for the reaction with pNP β-Glc catalyzed by AtBGlu42.
647 E and E-Glc represent AtBGlu42 (enzyme) and the glucosyl-enzyme intermediate, respectively. pNP-
648 Glc_2 is the transglucosylation product.
649

Figure 2. SDS-PAGE analysis of purified recombinant AtBGlu42.

Lane 1, protein size marker; Lane 2, purified tagged AtBGlu42 (1 μg); Lane 3, purified untagged AtBGlu42 (1 μg). Protein was stained with CBB. Molecular masses of the standard proteins are shown on the left. Recombinant tagged AtBGlu42 (70 kDa) and untagged AtBGlu42 (56 kDa) are indicated by an arrow.

Figure 3. Effects of pH and temperature on activity and stability of recombinant AtBGlu42.

(a) Relative activity at various pH (pH 4.1-11.0). (b) Relative activity at various temperatures (25-60 °C). (c) Residual activity after AtBGlu42 was kept in the pH range at 4 °C for 24 h. (d) Residual activity after AtBGlu42 was kept at the temperatures at pH 7.0 for 15 min. Values and error bars are average and standard deviation of three independent experiments, respectively.

Figure 4. Reaction of recombinant AtBGlu42 with pNP β-Glc.

(a, b) TLC analysis of the reaction of AtBGlu42 (2.27 μM) and 8 mM pNP β-Glc in 50 mM sodium phosphate buffer (pH 6.8) at 30 °C. Reaction products with pNP group were detected under UV light (a), and those containing sugar were detected by staining (b). (c) The s-*v* plots of the reaction of with pNP β-Glc. Velocity for aglycone release (circle), hydrolysis (triangle), and transglucosylation (square) are shown. (d) Transglucosylation ratio ($r_{tg} = v_{tg} / v_{ag}$) against pNP β-Glc concentration. Values and error bars are average and standard deviation of three independent experiments, respectively. Theoretical lines according to the kinetic scheme are drawn.

Figure 5. Crystal structure of AtBGlu42.

(a) Ribbon diagram of overall AtBGlu42. The structure is shown in rainbow coloring from blue (N-terminal) to red (C-terminal). Four glycerol molecules are shown in ball and stick representation. The extra N-terminal α-helix is located close to the small local domain composed β→α loops 5 (containing β-strand β5′ and α-helix α5′) and 6 (containing two β-strands β6′ and β6″). (b) Close up view of the active site of AtBGlu42. Two glycerol molecules observed are represented with balls and

sticks. Water molecules are shown as red balls. Predicted hydrogen bonds are indicated by dotted lines. The F_o-F_c omit electron density map for the glycerol molecules is shown as a mesh contoured at 3.5 σ.

Figure 6. Comparison of structure of AtBGlu42 with GH1 β-glucosidases.
(a) Superimposition of the residues at subsite −1 of AtBGlu42 (pink) with Os3BGlu7 (pale green), and Tmari_1862 (light purple). Inhibitors (glucoimidazole in Os3BGlu7 and Tmari_1862) are shown in ball and stick representation. (b) The Os3BGlu7-laminaribiose complex (PDB entry, 3AHT) (Chuenchor *et al.* 2011). (c) The corresponding part of AtBGlu42. Laminaribiose of the Os3BGlu7 complex superimposed with AtBGlu42 is shown. (d) The Os3BGlu7-cellopentaose complex (PDB entry, 3F5K) (Chuenchor *et al.* 2011). (e) The corresponding part of AtBGlu42. Cellopentaose of the Os3BGlu7 complex superimposed with AtBGlu42 is shown.

Figure 7. Docking simulation of scopolin onto AtBGlu42.
Scopolin is shown with balls and sticks. The amino acid residues surrounding it are shown behind transparent surface in grey for carbon. The umbelliferyl plane faces Trp360 and 6-methoxy group is at a distance of 3.4-3.8 Å from Phe197.

Figure 8. Comparison of the three-dimensional structures of AtBGlu42 and Td2F2.
(a) Arg342 and its surrounding structure of AtBGlu42. The ligand is cellopentaose from the Os3BGlu7 complex. (b) Corresponding Arg313 and structure of Td2F2 (PDB entry, 3WH5) (Matsuzawa *et al.* 2016). (c) Superposition of the small domain structures of AtBGlu42 (pink) and Td2F2 (purple). The small local domain composed of β→α loops 5 and 6 containing β-sheet (β5′, β6′, and β6″) is shown along with β-strands 5 and 6 and α-helices 5 and 6 of the $(\beta/\alpha)_8$-barrel. (d) View of the same local structure of AtBGlu42 from the right side. The hydrophobic core is observed between the small domain and α6. (e) The equivalent view of Td2F2. The hydrophobic core is not found, but possible salt-bridges between Asp244–Arg338 and Arg249–Asp264 are.

Table 1. Summary of crystallization conditions, data collection, and refinement statistics.

	AtBGlu42-Apo
Data collection	
PDB entry	7F3A
Beamline	SPring-8 BL41XU
Space group	$P2_1$
Unit cell parameters a, b, c, (Å)	44.7, 93.1, 60.9
Unit cell parameters α, β, γ, (º)	90, 102.5, 90
Wavelength (Å)	1
Resolution range (Å)	50.0-1.70 (1.80-1.70)
R_{meas} (%)[a]	8.1 (84.0)
$CC_{1/2}$	(0.783)
$\langle I/\sigma(I) \rangle$	15.1 (2.00)
Completeness (%)	99.9 (99.7)
Redundancy	6.76 (5.87)
Refinement	
No. reflection	53,471
R_{work}/R_{free} (%)[b]	16.0/18.0
No. of atoms	
Macromolecules	3,865
Ligand/ion	24
Water	402
B-factors (Å^2)	
Macromolecules	25
Ligand/ion	30.4
Water	34.6
RMSD from ideal	
Bond lengths (Å)	0.006
Bond angles (°)	0.796
Ramachandran	
Favored (%)	98.1
Allowed (%)	1.9
Outliers (%)	0

Values in parentheses are for the highest resolution shell.
a, $R_{meas} = \Sigma_{hkl} \{N(hkl) / [N(hkl) - 1]\}^{1/2} \Sigma_i | I_i(hkl) - \langle I(hkl) \rangle | / \Sigma_{hkl} \Sigma_i I_i(hkl)$, where $\langle I(hkl) \rangle$ and $N(hkl)$ are the mean intensity of a set of equivalent reflections and the multiplicity, respectively.
b, $R_{work} = \Sigma_{hkl} ||F_{obs}| - |F_{calc}|| / \Sigma_{hkl} |F_{obs}|$, R_{free} was calculated for 5% randomly selected test sets that were not used in the refinement.

Table 2. Reaction velocities and kinetic parameters of recombinant AtBGlu42 for various substrates.

Substrate	Reaction velocity [a] (s^{-1})	k_{cat} (s^{-1})	K_m (mM)	k_{cat}/K_m (s^{-1} mM^{-1})
pNP β-D-glucopyranoside	12.3 ± 0.2	10.2 ± 0.0 [b]	0.142 ± 0.002 [b]	72.2 [b] (71.9 [c])
pNP β-D-fucopyranoside	12.0 ± 0.0	12.9 ± 0.4	0.158 ± 0.004	81.3
pNP β-D-galactopyranoside	2.39± 0.04	13.6 ± 0.4	9.93 ± 0.41	1.34
pNP β-D-mannopyranoside	0.203 ± 0.003	0.233 ± 0.014	0.290 ± 0.005	0.804
pNP β-D-xylopyranoside	0.258 ± 0.002	0.464 ± 0.008	1.62 ± 0.04	0.287
pNP β-D-cellobioside	8.99 ± 0.95	9.40 ± 0.20	0.0978 ± 0.0028	96.1
4-Methylumbelliferyl β-D-glucopyranoside	8.03 ± 0.09	8.03 ± 0.08	0.0827 ± 0.0022	97.1
Scopolin	8.78 ± 0.01	10.2 ± 0.02	0.0981 ± 0.0001	104
Helicin	10.2 ± 0.3	10.5 ± 0.03	0.0657 ± 0.0044	160
Salicylic acid β-D-glucopyranoside	0.316 ± 0.014	N.D.	N.D.	N.D.
Arbutin	< 0.0046	N.D.	N.D.	N.D.
Phlorizin	0.418 ± 0.011	N.D.	N.D.	N.D.
Phenyl β-D-glucopyranoside	0.0897 ± 0.0046	N.D.	N.D.	N.D.
Methyl β-D-glucopyranoside	< 0.0046	N.D.	N.D.	N.D.
Octyl β-D-glucopyranoside	0.0254 ± 0.0027	N.D.	N.D.	N.D.
Cellobiose	2.00 ± 0.01	6.42 ± 0.09	4.07 ± 0.04	1.58
Cellotriose	9.99 ± 0.62	10.8 ± 0.1	0.126 ± 0.002	85.5
Cellotetraose	9.34 ± 0.31	10.3 ± 0.3	0.231 ± 0.01	44.7
Cellopentaose	8.59 ± 0.20	10.2 ± 0.2	0.283 ± 0.02	35.9
Cellohexaose	8.33 ± 0.15	9.67 ± 0.5	0.314 ± 0.02	30.8
Laminaribiose	10.6 ± 0.09	11.1 ± 0.2	0.117 ± 0.004	94.6
Laminaritriose	8.07 ± 0.35	10.7 ± 1.0	0.636 ± 0.09	16.9
Laminaritetraose	2.98 ± 0.29	N.D.	N.D.	1.68
Sophorose	8.35 ± 0.10	11.9 ± 0.2	0.864 ± 0.022	13.8
Gentiobiose	0.0593 ± 0.0040	0.543 ± 0.073	16.9 ± 3.1	0.032
Neotrehalose	< 0.0046	N.D.	N.D.	N.D.

Data are average ± standard deviation for three independent experiments. N.D., not determined. a, Reaction velocity to 2 mM substrates. b, Kinetic parameter of Michaelis-Menten equation determined in the low substrate concentration range (≤ 0.6 mM). c, k_{cat1}/K_{m1} of the kinetic model of retaining glycosidases that catalyze both hydrolysis and transglycosylation.

Table 3. Kinetic parameters of recombinant AtBGlu42 mutants for cellooligosaccharides.

Substate	R342A			R342Y		
	k_{cat} (s^{-1})	K_m (mM)	k_{cat}/K_m (s^{-1} mM^{-1})	k_{cat} (s^{-1})	K_m (mM)	k_{cat}/K_m (s^{-1} mM^{-1})
pNP β-D-glucopyranoside	7.89 ± 0.13 [a]	0.211 ± 0.008 [a]	37.5 [a]	1.35 ± 0.01 [a]	0.270 ± 0.005 [a]	4.98 [a]
Cellobiose	5.43 ± 0.16	4.82 ± 0.34	1.13	0.927 ± 0.044	10.8 ± 0.8	0.0855
Cellotriose	7.54 ± 0.13	0.136 ± 0.010	55.4	1.33 ± 0.03	0.323 ± 0.017	4.12
Cellotetraose	8.21 ± 0.05	0.122 ± 0.007	67.1	1.23 ± 0.01	0.109 ± 0.005	11.3
Cellopentaose	8.08 ± 0.11	0.107 ± 0.003	75.8	1.31 ± 0.04	0.127 ± 0.008	10.3
Cellohexaose	8.10 ± 0.22	0.151 ± 0.014	53.7	1.29 ± 0.03	0.147 ± 0.004	8.78

a, Kinetic parameter of Michaelis-Menten equation determined in the low substrate concentration range (≤ 0.6 mM).

Table 4. Subsite affinities for cellooligosaccharide.

	Subsite affinity (kJ mol^{-1})		
Subsite	Wild type	R342A	R342Y
−1	11.2 ± 0.1	11.6 ± 0.2	11.9 ± 0.2
+1	11.6 ± 0.1	11.0 ± 0.3	8.75 ± 0.27
+2	10.1 ± 0.0	9.83 ± 0.12	9.78 ± 0.06
+3	−1.64 ± 0.04	0.470 ± 0.083	2.54 ± 0.03
+4	−0.549 ± 0.059	0.304 ± 0.064	−0.246 ± 0.060
+5	−0.388 ± 0.081	−0.862 ± 0.106	−0.402 ± 0.034

The k_{int} of the wild type, R342A, and R342Y were 10.5 s^{-1}, 7.78 s^{-1}, and 1.31 s^{-1}, respectively.

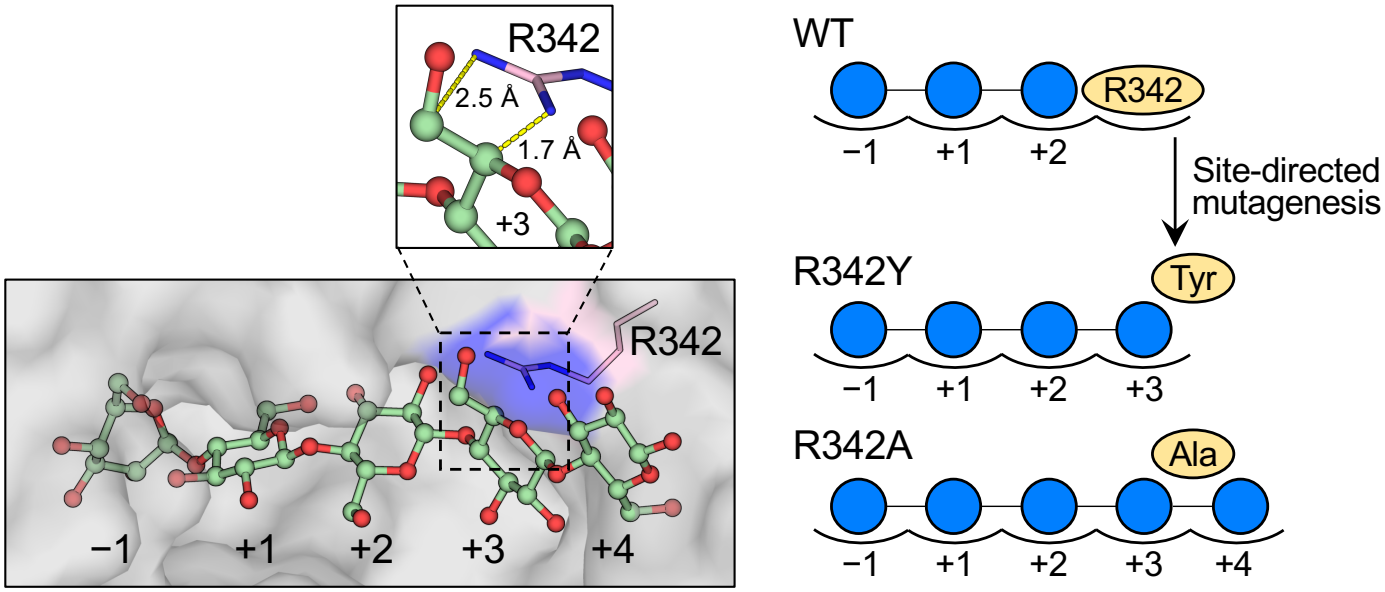

Graphical abstract. Horikoshi, et al.

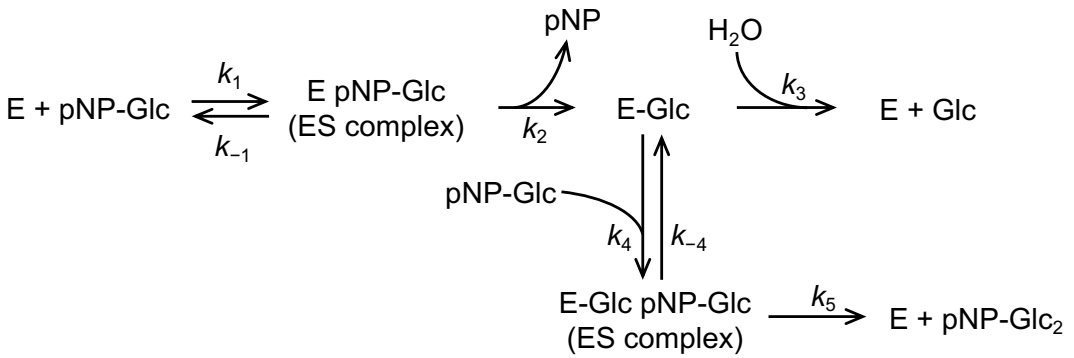

Figure 1. Horikoshi, et al.

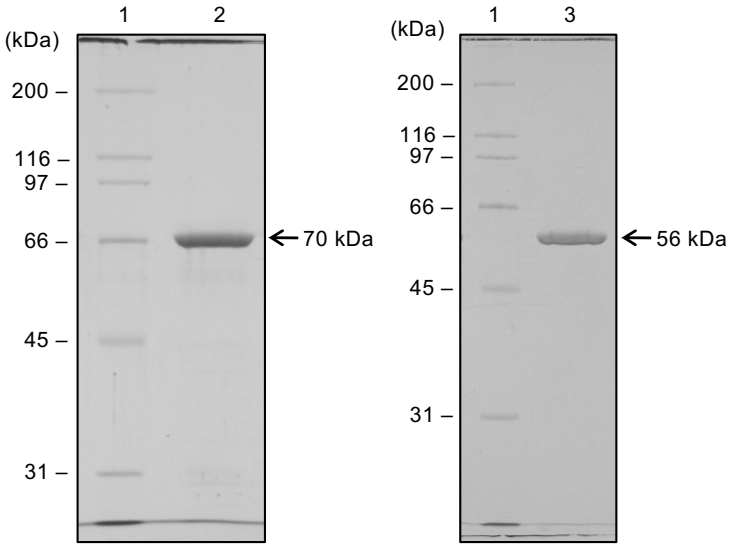

Figure 2. Horikoshi, et al.

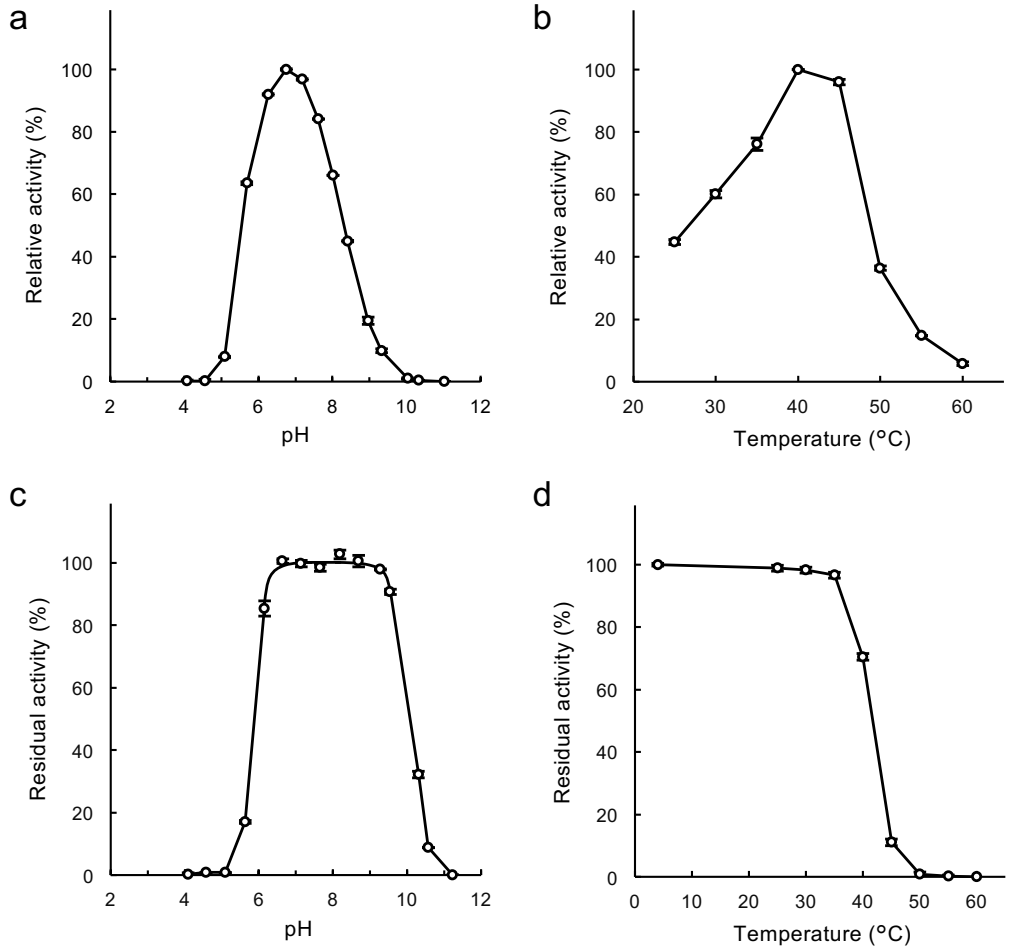

Figure 3. Horikoshi, et al.

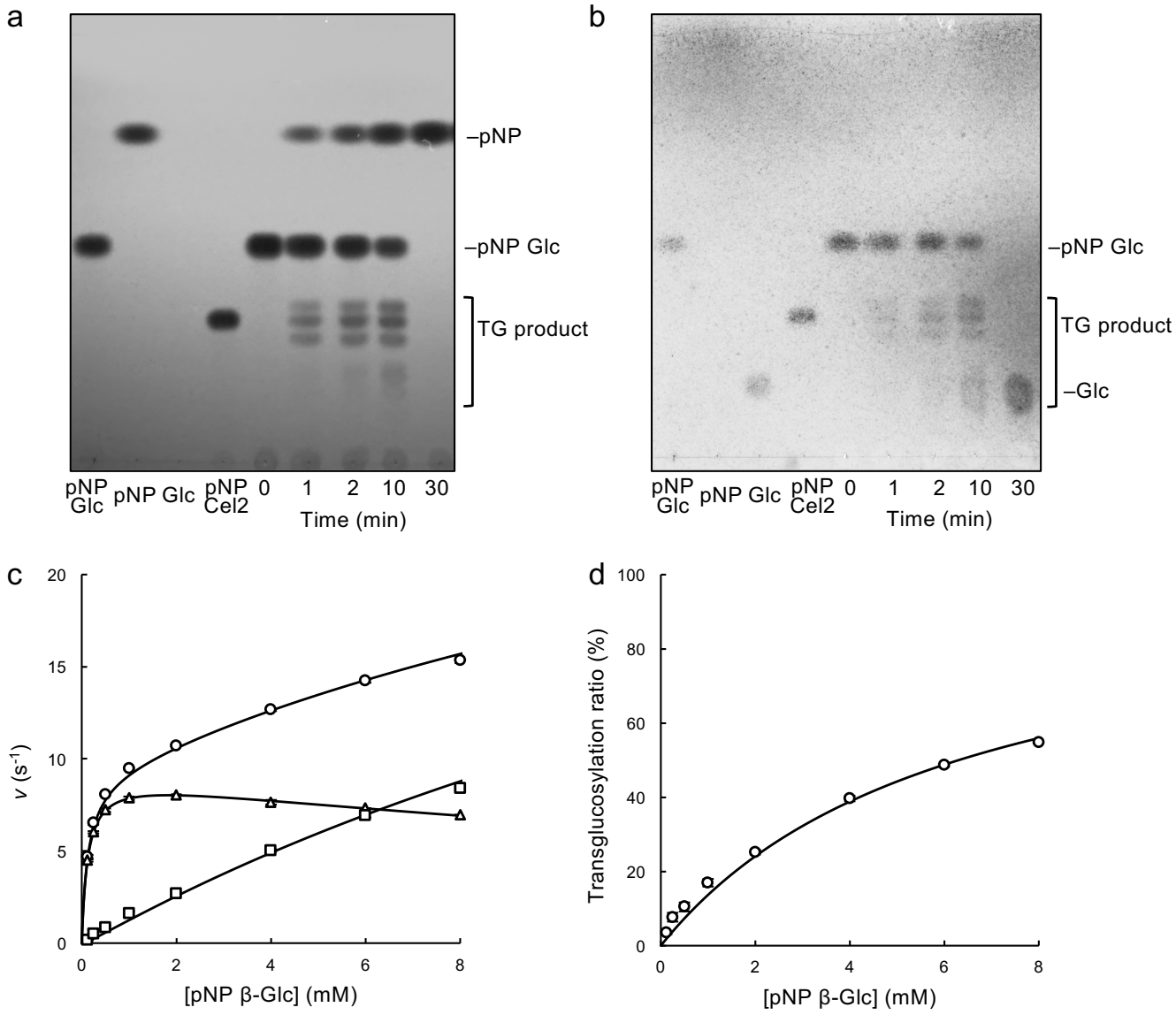

Figure 4. Horikoshi, et al.

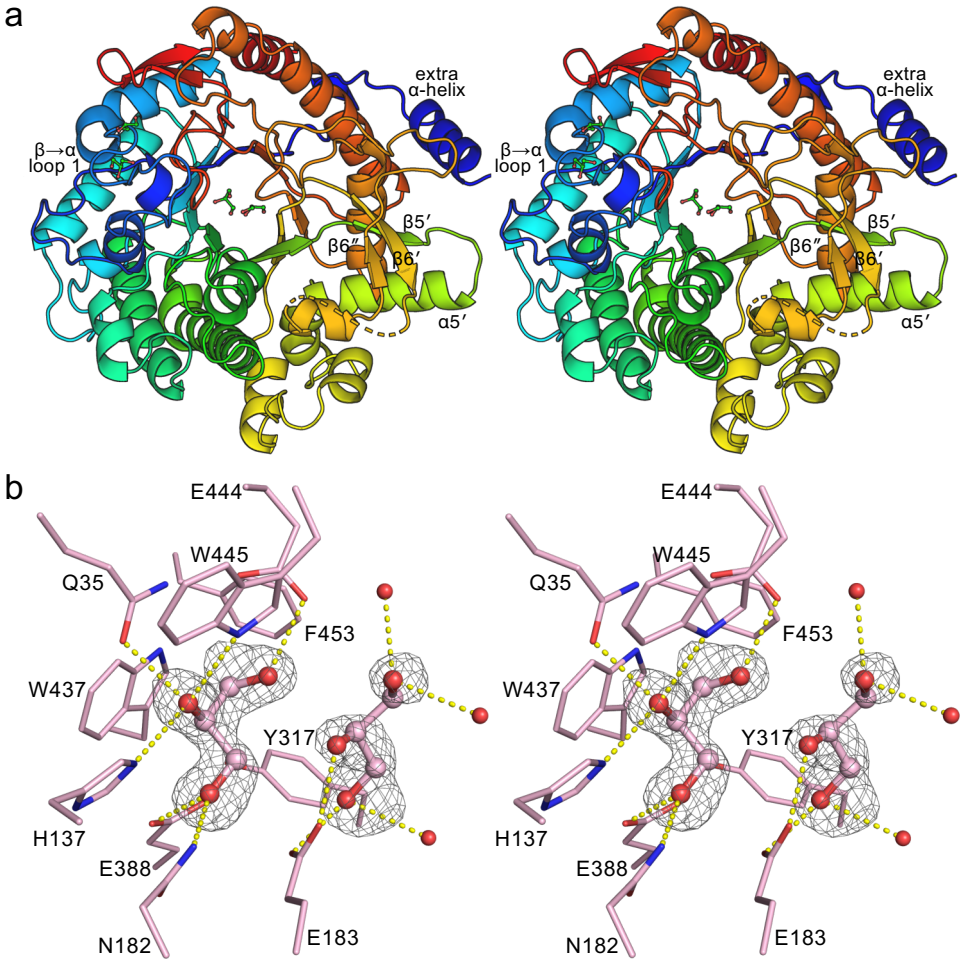

Figure 5. Horikoshi, et al.

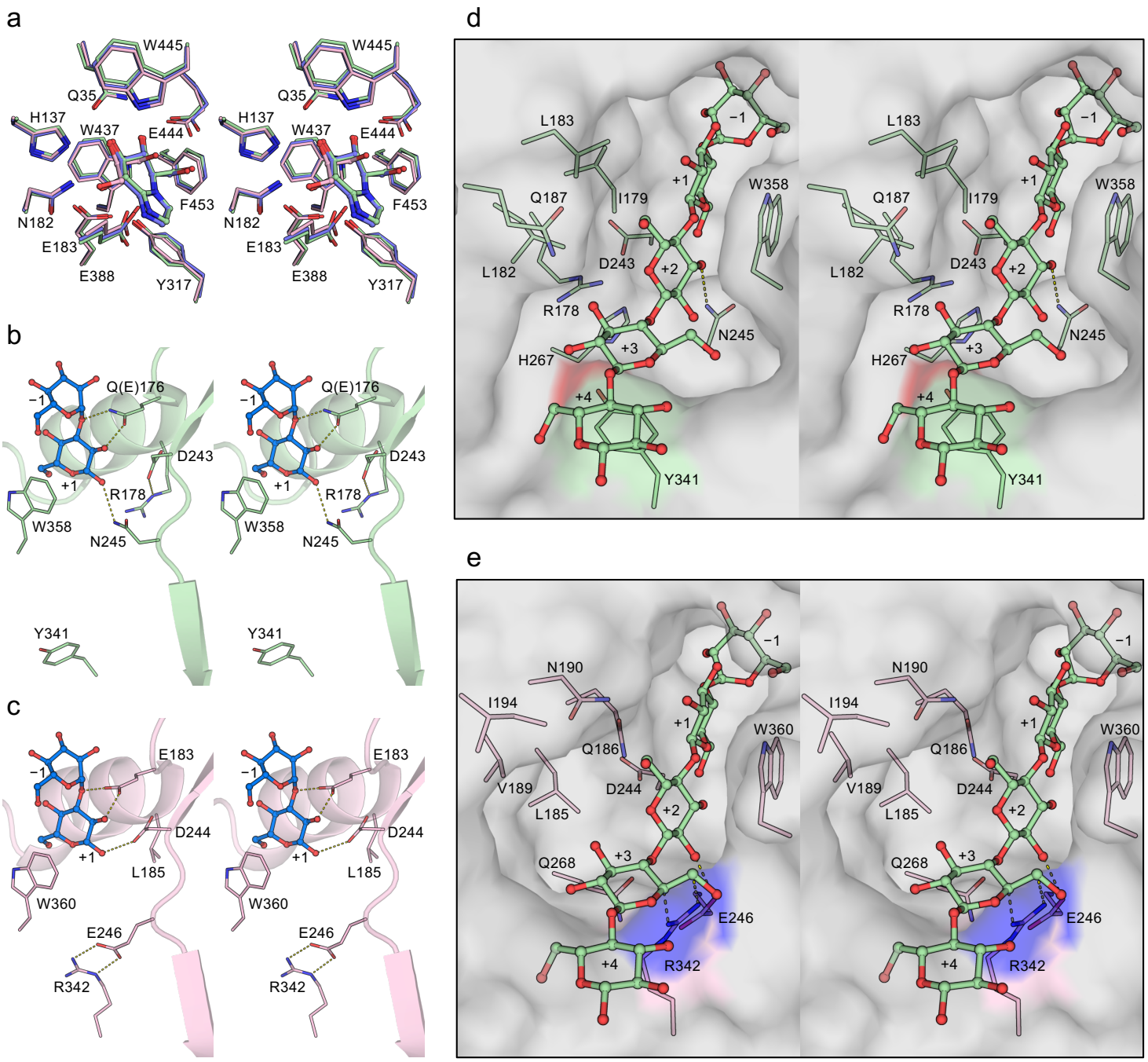

Figure 6. Horikoshi, et al.

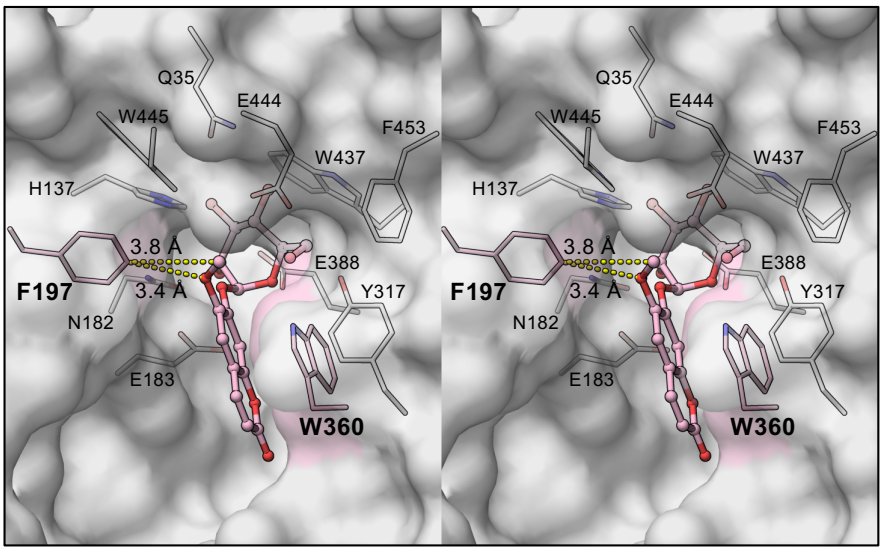

Figure 7. Horikoshi, et al.

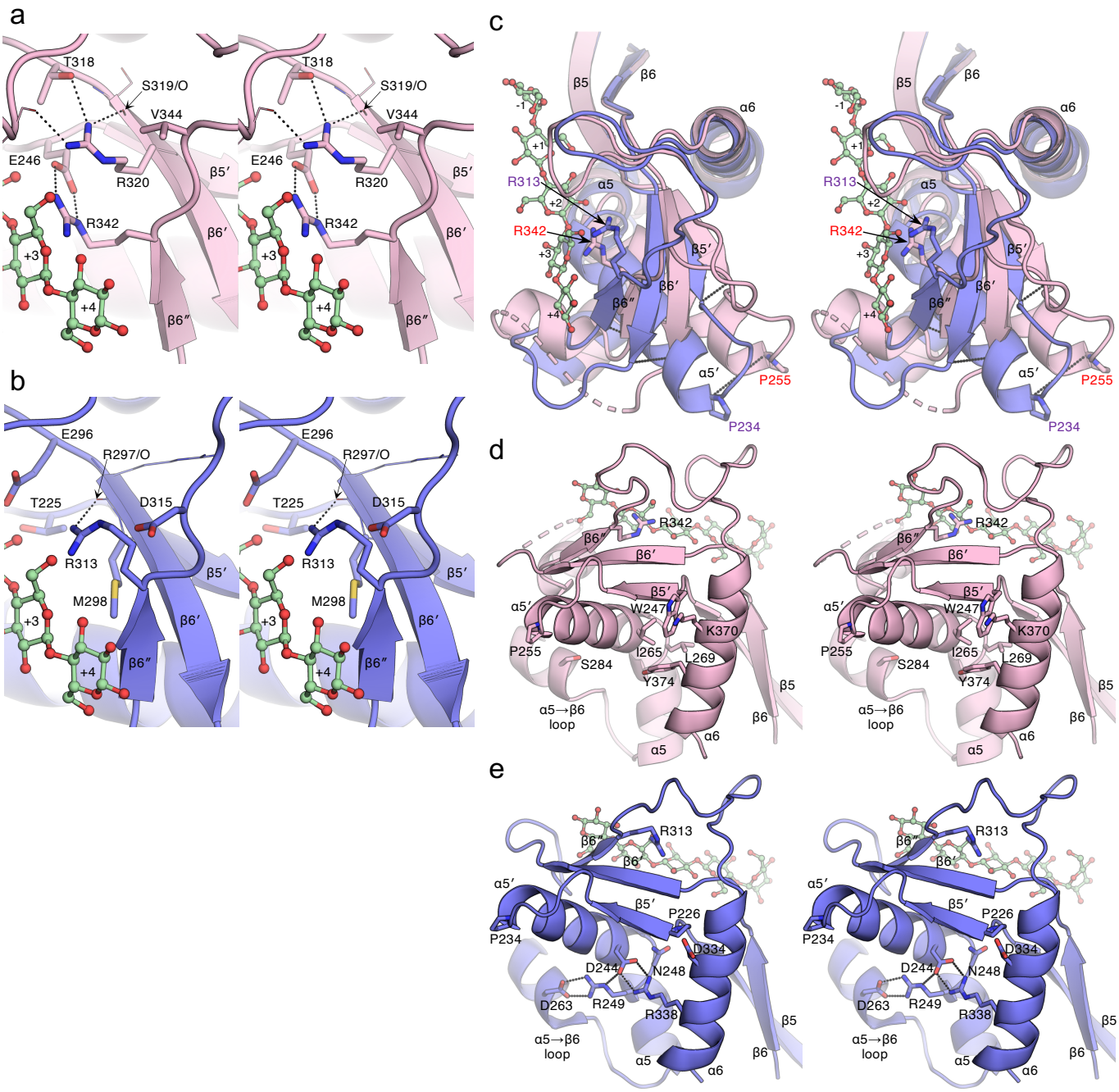

Figure 8. Horikoshi, et al.